Strong Linkage Between Observed Daily Precipitation Extremes and Anthropogenic Emissions Across the Contiguous United States

J S Nanditha, Gabriele Villarini, Hanbeen Kim, Philippe Naveau

Geophysical Research Letters

RESEARCH LETTER
10.1029/2024GL109553

Key Points:

- We apply the Extended Generalized Pareto Distribution for probabilistic event attribution to bypass issues with threshold specification
- Anthropogenic emissions alone could exacerbate the observed magnitude of extreme daily precipitation across the United States
- The study underscores the urgent need for mitigation, revealing a clear link between anthropogenic activities and extreme precipitation

Supporting Information:

Supporting Information may be found in the online version of this article.

Correspondence to:

J. S. Nanditha,
nanditha.js@princeton.edu

Citation:

Nanditha, J. S., Villarini, G., Kim, H., & Naveau, P. (2024). Strong linkage between observed daily precipitation extremes and anthropogenic emissions across the contiguous United States. *Geophysical Research Letters*, *51*, e2024GL109553. https://doi.org/10.1029/2024GL109553

Received 2 APR 2024
Accepted 4 OCT 2024

Author Contributions:

Conceptualization: Gabriele Villarini
Data curation: J. S. Nanditha
Formal analysis: J. S. Nanditha
Funding acquisition: Gabriele Villarini
Investigation: J. S. Nanditha, Gabriele Villarini, Philippe Naveau
Methodology: J. S. Nanditha, Gabriele Villarini, Philippe Naveau
Project administration: Gabriele Villarini
Software: J. S. Nanditha, Hanbeen Kim
Supervision: Gabriele Villarini
Visualization: J. S. Nanditha, Hanbeen Kim
Writing – original draft: J. S. Nanditha

Strong Linkage Between Observed Daily Precipitation Extremes and Anthropogenic Emissions Across the Contiguous United States

J. S. Nanditha[1,2], Gabriele Villarini[3,4], Hanbeen Kim[3,4], and Philippe Naveau[5]

[1]IIHR-Hydroscience and Engineering, University of Iowa, Iowa City, IA, USA, [2]Now at Department of Civil and Environmental Engineering, and High Meadows Environmental Institute, Princeton University, Princeton, NJ, USA, [3]Department of Civil and Environmental Engineering, Princeton University, Princeton, NJ, USA, [4]High Meadows Environmental Institute, Princeton University, Princeton, NJ, USA, [5]Laboratoire des Sciences du Climat et de l'Environnement, LSCE/IPSL, CNRS-CEA-UVSQ, Université Paris-Saclay, Gif-sur-Yvette, France

Abstract The results of probabilistic event attribution studies depend on the choice of the extreme value statistics used in the analysis, particularly with the arbitrariness in the selection of appropriate thresholds to define extremes. We bypass this issue by using the Extended Generalized Pareto Distribution (ExtGPD), which jointly models low precipitation with a generalized Pareto distribution and extremes with a different Pareto tail, to conduct daily precipitation attribution across the contiguous United States (CONUS). We apply the ExtGPD to 12 general circulation models from the Coupled Model Intercomparison Project Phase 6 and compare counterfactual scenarios with and without anthropogenic emissions. Observed precipitation by the Climate Prediction Center is used for evaluating the GCMs. We find that greenhouse gases rather than natural variability can explain the observed magnitude of extreme daily precipitation, especially in the temperate regions. Our results highlight an unambiguous linkage of anthropogenic emissions to daily precipitation extremes across CONUS.

Plain Language Summary We investigate how human-induced emissions affect daily rainfall extremes across the United States. The attribution of an extreme event to human-induced emissions depends on the selected extreme event statistics, with setting a threshold to define what counts as an extreme event remaining a major challenge. To overcome this, we used the Extended Generalized Pareto Distribution (ExtGPD) that jointly models both low and heavy rainfall events without defining a threshold, providing a more complete picture of the full distribution including extremes. We fitted the ExtGPD to 12 general circulation models and compared scenarios with and without human-induced emissions. Our findings suggest that human emissions are responsible for the observed intensity of daily rainfall extremes across the United States, especially in regions with temperate climates, and that these extremes would have been smaller without greenhouse gases.

1. Introduction

Climate attribution studies that examine the role of anthropogenic climate change in altering the probability of observed weather extremes have proliferated since Allen (2003), who proposed a simple probabilistic framework for attributing the role of anthropogenic forcing in the occurrence of an observed extreme. The availability of large ensemble climate model simulations and the Detection and Attribution Model Intercomparison Project (DAMIP) gave further impetus to climate attribution studies. The goal of these studies is to quantify the contribution of historic emissions and natural forcing in altering the risk of observed extremes and to project their changes (e.g., Gillett et al., 2016). This is generally accomplished using frequentist probabilistic methods (Oldenborgh et al. (2021) and references therein). Most of these studies are event-specific attribution of observed extraordinary weather extremes in recent years, while a few of them evaluate the role of anthropogenic emissions in altering the observed changes in extremes based on fingerprint techniques (e.g., Kirchmeier-Young et al., 2020; Risser et al., 2022).

Previous studies have reported an observed intensification of precipitation extremes in the central and eastern parts of the contiguous United States (CONUS) and no detectable change is reported in the western United States (Easterling et al., 2017; Guo et al., 2019; Trenberth, 2018). However, the existing event attribution studies have

Writing – review & editing: J. S. Nanditha, Gabriele Villarini, Hanbeen Kim, Philippe Naveau

reported a low to medium confidence in human attribution to observed precipitation extremes across the CONUS (Seneviratne et al., 2021). For instance, event attribution studies found that the 3-day rainfall that caused the Louisiana floods of 2016 had become 40% more likely since 1900 (Van Der Wiel et al., 2017) and extreme precipitation associated with Hurricane Harvey in August 2017 in Houston was intensified due to global warming (e.g., Wang et al., 2018; Wehner & Sampson, 2021; Zhao et al., 2018). Similarly, external forcing reportedly caused the intensification and increased frequency of 1-day and 5-day annual maximum precipitation across North America based on optimal fingerprinting techniques (Kirchmeier-Young et al., 2020). On the other hand, an unequivocal role of human forcing was not detected in the 2013 Colorado heavy rainfall events (Hoerling et al., 2013; Pall et al., 2017). Most of the existing attribution studies are based on specific observed precipitation extremes spanning a few days in duration and impacting a specific region of interest. Moreover, the use of different approaches in the extreme event definition and statistical modeling makes a direct comparison of these studies difficult.

The definition of extremes is an important criterion in determining the apparent role of anthropogenic climate change (e.g., Philip et al., 2020). Kirchmeier-Young et al. (2019) suggested that longer spatial and temporal scales increase the signal-to-noise ratio of extreme weather events, making it easier to attribute longer-than shorter-scale events to human influences. Statistical approaches used for extreme value analysis in climate attribution studies also influence the attribution statements (Naveau et al., 2020). The block maxima or peak-over-threshold (POT) approaches are usually employed to select the extreme events that are used for subsequent statistical modeling. While a block maxima approach reduces the sample size of observed extremes to one per year, the POT method is constrained by the arbitrary choice of the threshold (e.g., Nerantzaki et al., 2023). The threshold selection in a POT method represents a tradeoff between ensuring an adequate sample size for statistical testing and adhering to the assumptions of extreme value distributions. The different approaches in event definition and arbitrary choice of thresholds make it difficult to interpret the existing studies. This necessitates the use of statistical approaches that are not dependent on threshold specification for climate attribution studies.

To address this issue, we employ the Extended Generalized Pareto distribution (ExtGPD; Naveau et al., 2016), which jointly models low precipitation with a GPD and heavy rainfall with a different Pareto tail, for building the statistical framework for climate attribution. The ExtGPD helps in modeling the entire range of data without the need for specifying a threshold, thereby increasing the sample size needed for fitting the statistical model. Here, we use the ExtGPD for providing a comprehensive statement on the role of anthropogenic forcing on altering the risk of daily precipitation extremes by sampling the entire precipitation time series across CONUS. We use counterfactual simulations from 12 general circulation models (GCMs) that participated in the DAMIP of the 6th Coupled Model Intercomparison Project (CMIP6) for generating the attribution statements. We organize the study into three sections: (a) evaluation of the performance of the GCMs in capturing daily precipitation extremes; (b) attribution of human contributions to daily precipitation extremes by comparing historical simulations with counterfactual scenarios based on n-year return level extremes; and (c) estimation of the sensitivity of anthropogenic forcing to the magnitude of extremes and climatic regions.

2. Data and Methods

2.1. Data

We used daily precipitation by the Climate Prediction Center (CPC) available at 0.25° resolution over CONUS. For the evaluation and attribution study, we used 12 CMIP6 GCMs (Table S1 in Supporting Information S1) simulations from hist-nat, hist-GHG and historical scenarios. The hist-nat simulations are based on natural forcing (solar irradiation and volcanic aerosols) and exclude anthropogenic forcing (anthropogenic aerosols and emissions). The hist-GHG simulations are forced by well-mixed greenhouse gas emissions and exclude both natural and anthropogenic aerosols. The historical scenarios of GCMs are based on anthropogenic (GHG and aerosols) and natural forcing (volcanic and solar). The DAMIP GCMs are forced from 1850 to 2014 (Gillett et al., 2016). We used 34-year simulations from 1981 to 2014 to focus on the most recent decades and to mitigate potential issues related to the presence of non-stationarities. We regridded the CPC daily precipitation and climate model simulations to 1-degree resolution using bilinear interpolation to ensure consistency among the data sets. We excluded daily gridded precipitation below 0.1 mm of both CPC and CMIP6 data sets for the analysis to remove drizzle bias in the GCMs (e.g., Dai, 2006; DeMott et al., 2007).

2.2. Methods

2.2.1. Extreme Value Modeling

The generalized Pareto distribution (GPD) family is widely used for modeling extreme precipitation exceeding a particular threshold as it is appropriate for modeling heavy tail distributions (e.g., Coles, 2001) (Equation 1); however, the threshold selection is challenging. A large threshold could reduce the sample size and leads to higher uncertainty in the parameter estimations, while a smaller threshold does not satisfy the approximations of the GPD leading to model errors (e.g., Rivoire et al., 2021; Serinaldi & Kilsby, 2014). Naveau et al. (2016) proposed a transition function to the GPD that provides a smooth connection between the upper tail and the main body of the function. This approach, called the extended GPD (ExtGPD), avoids the need for threshold specification and helps in sampling the entire timeseries for modeling extremes. This approach has been applied and tested in various contexts (e.g., Gamet & Jalbert, 2022; Haruna et al., 2023; Legrand et al., 2023; Rivoire et al., 2021).

The probability distribution of the GPD when the shape ξ (upper tail parameter) is larger than zero (i.e., heavy tail behavior) is:

$$H\left(x/\sigma\right) = 1 - \left(1 + \frac{\xi x}{\sigma}\right)^{-1/\xi} \text{ for } \xi > 0 \tag{1}$$

where, σ is the scale parameter of the GPD and x is a scalar in the support of H.

The ExtGPD is a transformation of the GPD, such that:

$$G(v) = v^k \text{ ; where } v = H\left(x/\sigma\right) \tag{2}$$

and $k > 0$ is the lower tail parameter.

Naveau et al. (2016) proposed four different statistical formulations for the extended GPD model. We use the ExtGPD with three parameters (i.e., scale, lower tail parameter and the shape or upper tail parameter) owing to its simplicity and convergence of the statistical framework (Equation 2). We estimate the parameters using the probability weighted moments method as it converges better than the maximum likelihood estimation (Naveau et al., 2016). We use the following initial values for the parameters: shape $\xi = 0.2$; scale, $\sigma = 1$; lower tail parameter, $k = 0.5$. We fit the ExtGPD to CPC and GCM daily precipitation values above 0.1 mm for each 1-degree grid and estimate daily precipitation extremes of various return periods.

We compared the shape parameters of the ExtGPD and GPD for three different POT thresholds (Figure S1 in Supporting Information S1) since the shape parameter of a distribution is crucial in the determination of extreme values. We observed that the shape parameter of the ExtGPD follows the spatial pattern of extreme precipitation, with a median value of 0.25 ([0.21; 0.30] as the 95% confidence intervals). The GPD shape parameter is sensitive to the record length and the selected threshold. Higher POT thresholds result in a low sample size and lead to increased uncertainty in the estimation of the shape parameter, for instance, the range of GPD shape parameter for a POT threshold of 99th percentile is in the interval (−0.27,0.37; Figure S1 in Supporting Information S1) (Alonso et al., 2014; Serinaldi & Kilsby, 2014). The result of the comparison provides a strong case for the use of the ExtGPD in place of GPD as the former bypasses these limitations. Although there is an apparent bias in the shape parameter estimates between the GPD and ExtGPD approaches, it is noteworthy that the GPD confidence intervals for higher POT thresholds (98th and 99th percentiles) contain the ExtGPD interval (Figure S1 in Supporting Information S1). So, for higher thresholds, it will be difficult to reject the hypothesis that shape parameter estimates of GPD and ExtGPD are equal. More importantly, in the present study we focus only on comparisons across different climate scenarios, and the relative bias in ExtGPD shape parameter with respect to the GPD shape parameter is expected to remain constant and not impact our results.

We evaluate the performance of the GCMs in simulating observed precipitation based on the ability of the historical GCM simulations to capture CPC precipitation extremes: for each grid, we select only those models whose n-year return level of precipitation in historical simulations falls within the 95% confidence interval (CI) of

the n-year return level of the CPC observations. Thus, we identify a subset of good-performing GCMs for each grid, which we use in the subsequent event attribution.

2.2.2. Climate Attribution of Extreme Precipitation

We use the 34-year counterfactual scenarios of hist-nat and hist-GHG (1981–2014) from the subset of GCMs to make a probabilistic attribution statement. We estimated the ratio of change in the return level of extreme precipitation of the counterfactual scenarios to that of the historical simulations to quantify the impact of anthropogenic emissions (Equation 3).

$$\text{Attribution Ratio} = \frac{P_{\text{Counterfactual}} - P_{\text{historical}}}{P_{\text{historical}}}, \tag{3}$$

where counterfactual stands for both hist–nat and hist–GHG. We reiterate that the hist-nat simulations are forced by natural forcing and the hist-GHG simulations are forced by well mixed greenhouse gases alone.

A ratio greater (smaller) than zero implies that the counterfactual scenario increases (decreases) the n-year return level precipitation compared to the historical forcing. Further, we evaluate the sensitivity of the attribution ratio to different return periods and climate zones. The CONUS mainly falls within three climatic zones: arid, temperate and cold as per the Köppen-Geiger climate classification (Beck et al., 2018). We separately assess the attribution ratio for each of the three climate zones. The analysis for the ExtGPD is performed in R using the mev and gmm libraries (Belzile et al., 2015; Chaussé, 2010).

3. Results

3.1. Evaluation of CMIP6 GCMs

We validated the performance of the GCMs by comparing their ability to capture the observed extremes. The spatial pattern of extremes is well captured by CESM2, CanESM5, E3SM-2-0, FGOALs-g3 and MRI-ESM2-0 (Figure 1b). The largest values in precipitation extremes based on CPC (Figure 1a) tend to be concentrated along the Gulf Coast and to decrease as we move inland northward, and on the Sierra Navada in the west; most GCMs can capture this gradient, even though some of them fail to do so. For instance, ACCESS-CM2, ACCESS-ESM1-5, BCC-CSM2-MR, GFDL-ESM4 and MIROC6 overestimate extremes in the central part of the study region. Despite being comparatively better, E3SM-2-0 and FGOALS-g3 slightly underestimate precipitation extremes in the west-central regions and CanESM5 underestimates extremes along the Gulf Coast. We observed the GCMs to perform well in simulating the extreme rainfall patterns in the U.S. Northeast, West Coast, the Great Plains of the North and South, and southeastern regions, which receive relatively high extreme precipitation (Figure 1). We also examined the performance of GCMs in capturing higher return level precipitation (Figures S2–S4 in Supporting Information S1) and found similar spatial patterns to those in the 100-year return period. Overall, most GCMs capture the spatial pattern of extreme precipitation across CONUS, even though a few of them overestimate extremes, limiting their use in subsequent modeling.

Srivastava et al. (2020) evaluated the performance of CMIP6 GCMs in capturing precipitation extremes across CONUS. They found MRI-ESM2-0 and IPSL-CM6A-LR tend to overestimate total annual precipitation in the western CONUS, while BCC-CSM2-MR and CESM2 show a dry bias in the central Great Plains. The underestimation of precipitation in the central Great Plains is in general attributed to the poor convective parametrization, which fails to represent the mesoscale convective systems active in this region (e.g., Na et al., 2022). The wet bias in the U.S. Southwest is attributed to the higher number of wet days in certain GCMs, resulting in higher total annual precipitation. We observe MRI-ESM2-0 and IPSL-CM6A-LR show wet (dry) bias of daily precipitation extremes along the U.S. West Coast (U.S. Southeast), consistent with their findings. On the contrary, BCC-CSM2-MR overestimates extremes in the central Great Plains. Evaluation of GCMs depends on the assessment period, evaluation metrics and the GCMs considered, resulting in potentially contrasting findings. We find both wet and dry biases in daily precipitation extremes in different regions across CONUS, supporting and contradicting existing studies (Srivastava et al., 2020; Wang and Asefa, 2024).

To mitigate issues with the biases in the estimates of extremes in certain GCMs, for attribution we considered only those models whose n-year precipitation falls within the 95% CI of the observations for each grid (Figure 1b). This

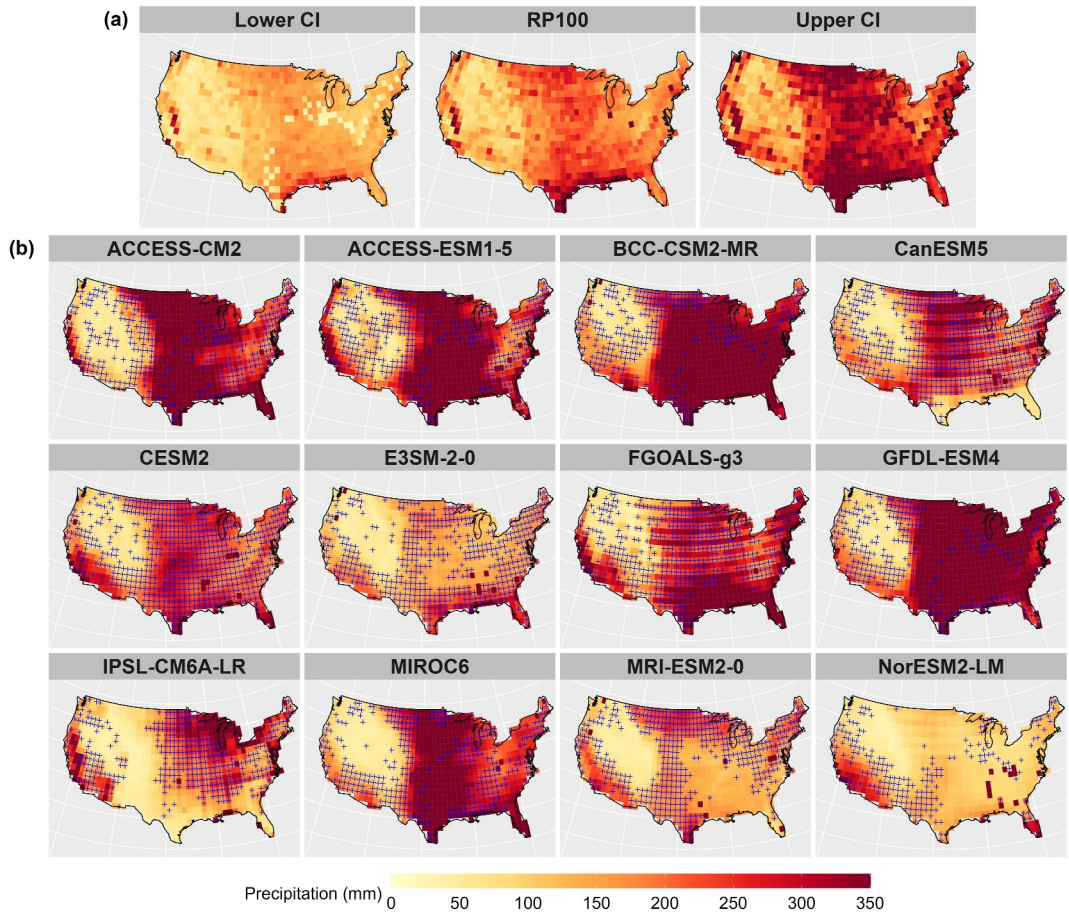

Figure 1. Evaluation of GCMs. Panels (a) show the 100-year daily precipitation (mm) and their upper and lower confidence interval (CI) (95% CI) based on Climate Prediction Center (CPC) observations from 1981 to 2014. Panels (b) show the 100-year daily precipitation extremes for the 12 GCMs from 1981 to 2014. The blue crosses highlight the grids that fall within the 95% CI of the CPC observations.

approach helps in removing the GCMs that significantly underestimate or overestimate the observed precipitation pattern, helping to reduce the uncertainty in climate attribution statements. More than five GCMs satisfy the above condition in most grids across CONUS, with the highest number of GCMs available in the western and central United States, as well as the northeastern regions (Figure S5 in Supporting Information S1). At least three GCMs with satisfactory performance are available in more than 87% grids (730 grids of the total 831 grids) across CONUS, thereby ensuring the robustness of the estimates. In short, over five GCM simulations of n-year return level precipitation are consistent with the corresponding CPC simulation of precipitation extremes across most of the CONUS and we use them for climate attribution (Figure S5 in Supporting Information S1). Moreover, the whole time series of precipitation (>0.1 mm) are sampled by fitting the ExtGPD distribution. Therefore, the comparison of extremes in CMIP6 GCMs and CPC observations provides more confidence in the GCM precipitation simulations.

3.2. Climate Attribution

We estimate the attribution ratio by taking the ratio of the change in return level in the counterfactual scenario (hist-nat and hist-GHG) to that of the historical simulations (Equation 3). We estimate the multi-model mean attribution ratio of the subset of GCMs that performed well compared to CPC for each grid based on 100-year precipitation (Figure 2 and Figures S6 and S7 in Supporting Information S1). Most regions across the country exhibit an attribution ratio below 0 in the hist-nat scenario and above 0 in the hist-GHG scenario (Figure 2). The results show a counterfactual scenario of natural-only forcing would have made the 100-year daily precipitation event smaller than the observations (Figure 2). Likewise, a well-mixed greenhouse gas emission scenario that

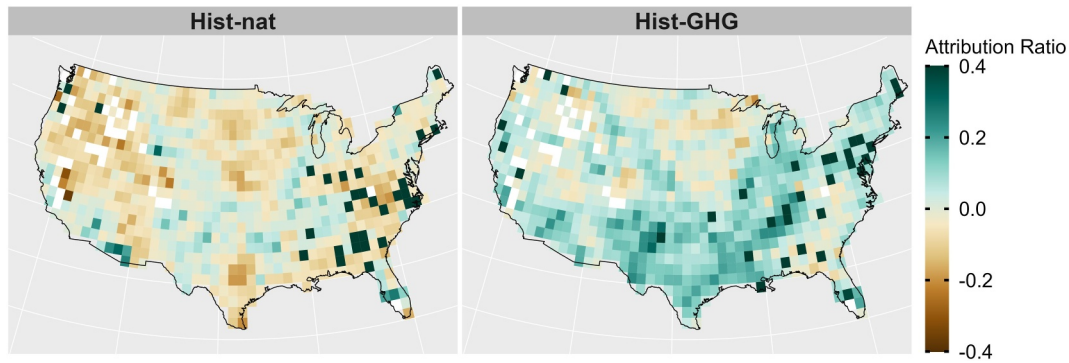

Figure 2. Multi-model mean attribution ratio of hist-nat and hist-GHG simulations estimated using the subset of GCMs that performed well with respect to Climate Prediction Center for the 100-year daily precipitation. For each grid, the mean is estimated based on the GCMs that capture the observed extremes (Figure S5 in Supporting Information S1). The white color corresponds to grids for which all GCMs failed to capture the observed extremes within the 95% confidence interval.

excludes both anthropogenic and natural aerosols would have enhanced the 100-year daily precipitation extremes during the observational period (Figure 2). We observed consistent patterns in the attribution ratio at higher return levels of daily precipitation (Figure S8 in Supporting Information S1). Overall, we identify the significant role of anthropogenic emissions in exacerbating the daily precipitation extremes across CONUS.

We also determined the 95% CI of the attribution ratio for 100-year precipitation extremes using 1000 bootstrap samples (Paciorek et al., 2017). Our analysis revealed that the lower and upper confidence bounds for both scenarios often fall below and above zero, respectively, resulting in overlapping confidence bounds for most grids (Figures S9 and S10 in Supporting Information S1). Therefore, we conducted a Kolmogorov-Smirnov (KS) test between the attribution ratios of hist-nat and hist-GHG scenarios for each GCM and the multi-model mean, considering only the grids where the GCM historical simulations fall within the CPC observations. We found a significant difference ($\alpha = 0.05$) in the distribution of the attribution ratios for both scenarios for all 12 GCMs (Table S2 in Supporting Information S1). Furthermore, the KS test between the extreme precipitation magnitudes for the historical and counterfactual scenarios shows a significant difference ($\alpha = 0.05$) between historical and hist-GHG scenarios for the majority of GCMs and the multi-model mean for all return levels (Table S3 in Supporting Information S1). However, significant differences in precipitation magnitudes are not observed in the case of hist-nat simulations.

Five or more GCMs that capture the historical extremes are considered for computing the multi-model mean attribution ratio in most grids (Figure S5 in Supporting Information S1). We compared the sign of the attribution ratio of the subset of GCMs in each grid to assess the robustness of the estimates of different GCMs. The majority of the GCMs show a negative sign of change in the hist-nat scenario and a positive sign of change in the hist-GHG scenario (Figures S6–S8 in Supporting Information S1). We found that a high percentage of GCMs agree in the sign of change at regions with high strength in attribution (Figure 2 and Figure S11 in Supporting Information S1). The Northwest, U.S. East Coast, Midwest and southern regions show a high negative attribution ratio and have a high percentage of GCMs agreeing on the sign of change (negative attribution ratio) in the hist-nat scenario (Figure 2 and Figure S11 in Supporting Information S1). Similarly, the Southern Plains, the east-central United States, U.S. Northeast and West Coast show high positive attribution ratio and have a higher percentage of GCMs agreeing on the positive sign of change (Figure 2 and Figure S11 in Supporting Information S1). Thus, the grids with higher magnitude of the multi-model mean attribution ratio have more GCMs that agree on the sign of change, making the result robust across the GCMs. The higher magnitude of extreme precipitation in a GHG-only scenario (hist-GHG) compared to the historical simulations highlights the modulating effect of natural and anthropogenic aerosols in reducing precipitation intensities. Aerosols, particularly sulfate aerosols, have a net negative impact on radiative forcing due to their high reflectance and indirect effect on cloud formation, leading to a reduction in precipitation (e.g., Allan et al., 2020; Risser et al., 2022). The positive attribution ratio in the hist-GHG also coincides with regions with high sulfate aerosols emissions across CONUS, including the northeastern, the east-central and southwestern United States and the U.S. West Coast (Risser et al., 2022). The increased risk of extreme daily precipitation in the hist-GHG scenario can be attributed to not accounting for the role of aerosols. A

lower daily precipitation magnitude in the natural-forcing scenario emphasizes the role of GHG emissions in exacerbating the precipitation extremes. We have not directly compared the precipitation magnitudes in the two counterfactual scenarios of well-mixed GHG and natural only forcing. However, it is evident that GHG forcing alone would have enhanced the magnitude of observed extremes compared to natural forcing (Figure 2 and Figures S6–S8 in Supporting Information S1).

We observed distinct regional patterns in the attribution ratio. The Southern Plains, east-central and north-eastern United States, which receive intense precipitation, exhibit a higher sensitivity of precipitation extremes to anthropogenic forcing (right panel in Figures 1a and 2). On the contrary, the western United States, including the U.S. Northwest and the Northern Plains, show a higher reduction in extremes under natural-only forcing (left panel in Figure 2). This is consistent with the spatial pattern of observed extreme precipitation across CONUS (Figure 1a). An intensification of heavy precipitation is observed since 1979 in the central and eastern United States, attributed to the increased frequency of mesoscale convective systems that cause heavy precipitation during the warm season (Easterling et al., 2017). Similarly, a linear increase in precipitation extremes is reported in the Midwest, U.S. East Coast and the Great Plains excluding the northwest regions (Dong et al., 2021), with a low confidence in the increase of extreme precipitation in the western regions (Seneviratne et al., 2021). Overall, we found the Southern Plains and the northeast regions, which receive intense daily precipitation and an observed increase in extremes, are highly sensitive to anthropogenic GHG emissions, more so than some of the drier northwestern regions.

3.3. Role of Climate Patterns and Return Period on the Attribution Ratio

We observed regional variability in the attribution ratio under the two counterfactual scenarios. To understand the role of climatic regions on the attribution ratio, we estimated the multi-model mean attribution ratio for the three major Köppen-Geiger climate classes over CONUS, namely arid, cold and temperate regions (Beck et al., 2018). The temperate regions exhibit the highest increase in extreme precipitation under hist-GHG simulations, followed by the arid regions, with the areas belonging to the cold region showing the lowest signal (Figure 3). The vast number of event attribution studies conducted in the southern and central United States highlights the role of anthropogenic emissions in increasing the probability of observed precipitation extremes in the temperate eastern United States (Van Der Wiel et al., 2017; Wang et al., 2018; Zhao et al., 2018), consistent with our findings. In the hist-nat scenario, the temperate and arid regions show a relatively low decrease in precipitation extremes compared to the cold regions, which show the highest decrease (Figure 3). Moreover, the cold regions have the smallest interquartile spread in the attribution ratio in the hist-nat scenario. However, the difference among the climatic regions is much less in hist-nat compared to hist-GHG scenario. As observed earlier, the arid and cold regions, which received low precipitation extremes during the study period, have a low attribution ratio compared to the temperate regions in the hist-GHG scenario, which receive intense daily precipitation. This implies that GHG emissions exacerbate precipitation extremes in wetter regions compared to drier ones.

We also compared the sensitivity of the attribution ratio to the magnitude of the extremes. We observed a slight increase in the risk of extreme precipitation of higher return periods (RP = 200, 250, 500) due to anthropogenic emissions (Figure 3 and Figures S8 and S12 in Supporting Information S1). There is a nominal increase (decrease) in the multi-model mean attribution ratio in the hist-GHG (hist-nat) scenario with an increase in precipitation return period (Figure 3 and Figure S12 in Supporting Information S1). However, there is a substantial increase in the interquartile range as the return period increases (Figure 3 and Figure S12 in Supporting Information S1). The temperate climatic regions exhibit a relatively higher increase in the attribution ratio in the hist-GHG scenario compared to the hist-nat (Figure 3). Overall, we find that the likelihood of higher magnitude precipitation extremes would have increased in a counterfactual scenario of anthropogenic emissions alone compared to the historical scenario. Previous studies outline that the probability of rare extremes increases at a higher rate in a warming world (Myhre et al., 2019), in agreement with our results, even though at a more muted level.

4. Discussion and Conclusions

We used the ExtGPD to assess the performance of 12 DAMIP GCMs in capturing the daily precipitation extremes. Unlike the GPD, the ExtGPD samples the entire time series and removes the arbitrariness in threshold selection in modeling extremes. Hence, the comparison of CPC observations and GCMs using the ExtGPD provides a robust estimation of the climate model performance, and we found that most GCMs capture the spatial

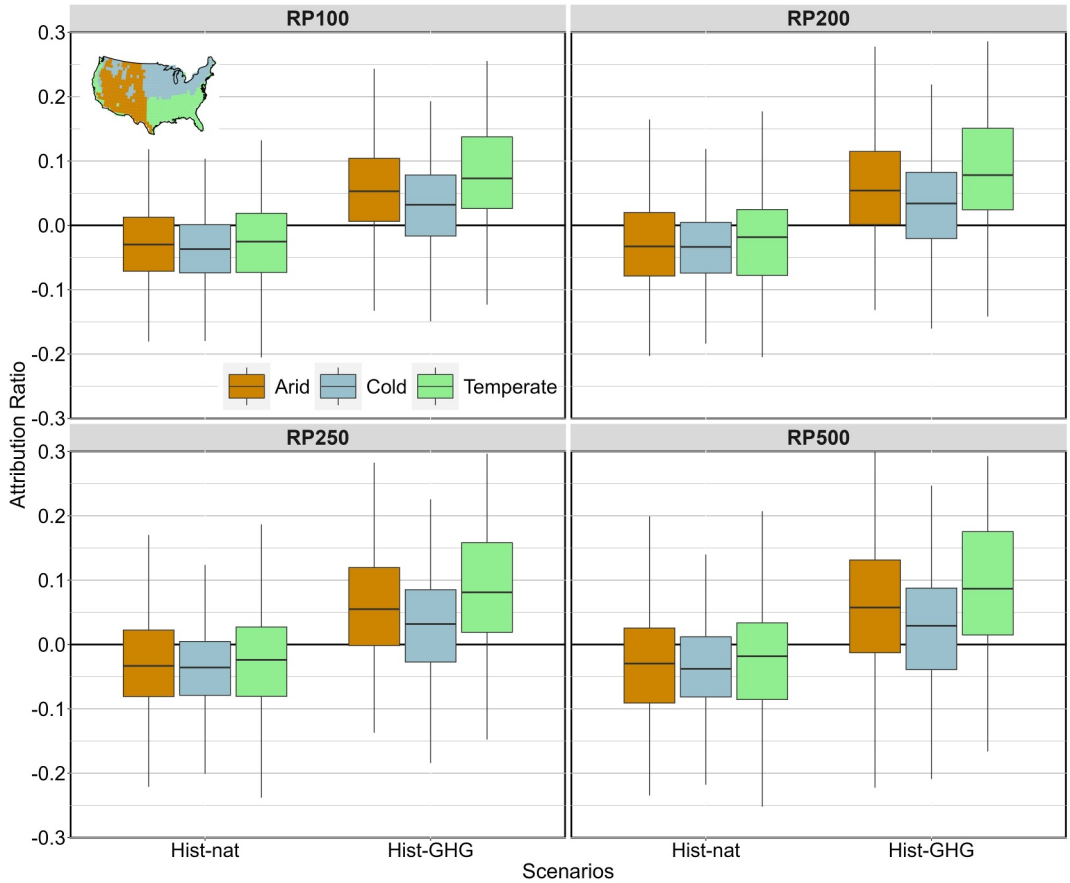

Figure 3. Attribution ratio for the three main Köppen-Geiger climate classes across CONUS. The spatial extent of the three main climate classes (arid, cold, and temperate) is shown in the inset figure. The box plots depict the attribution ratio for the three climate classes in a hist-nat and hist-GHG scenario for 100, 200, 250, and 500-year daily precipitation. In the boxplots, the dark horizontal line represents the median, the box represents the interquartile range, and the whiskers correspond to the 5th and 95th percentile values.

pattern of observed extremes. Our probabilistic attribution study shows an unambiguous connection of human emissions to daily precipitation extremes across CONUS. We report higher confidence in the attribution of daily precipitation extremes to well-mixed GHG emissions in the Northeast, Southern Plains, east-central United States, and U.S. West Coast, which receive high extreme precipitation, consistent with previous studies (e.g., Dong et al., 2021; Easterling et al., 2017). The arid regions in the west and the colder Midwest show a higher sensitivity to a counterfactual scenario of natural forcing, implying a reduction in extreme precipitation magnitude compared to the observed extremes. The spatial distribution of the attribution ratio identified in the study aligns with the observed pattern of precipitation extremes, suggesting a tendency for increased extreme magnitudes in regions experiencing higher levels of extremes. The Fifth US National Climate Assessment report highlights a relative increase in total annual precipitation in the Great Plains and eastern CONUS, and an increase in extreme precipitation in the eastern CONUS in the early 21st century relative to the first half of the 20th century (Marvel et al., 2023). Our attribution results highlight the increased role of GHG emissions in exacerbating the observed precipitation extremes in northeastern and east-central CONUS.

One limitation of this study is the lower spatial resolution of the DAMIP GCMs (~120 km), which leads to an inherent disadvantage in the accurate simulation of the regional precipitation patterns. However, the attribution ratio defined in the study is based on the counterfactual scenarios of the same climate models forced with different external forcings. Therefore, assuming that the response of the GCMs to the anthropogenic and natural forcing would be the same across resolutions, then our attribution statements would not be impacted by their coarse resolution. This assumption should be verified in future studies using a suite of models with different resolutions. To strengthen our results and lend more credence to their robustness, we only considered a subset of GCMs that

performed well in reproducing the observed statistical properties of rainfall extremes, and used the ExtGPD, which samples the entire time series with no need for thresholds. We conducted our analysis for the annual precipitation time series. However, future research could benefit from examining each season separately as the processes that cause extreme precipitation vary across seasons and could provide insights into the variations in precipitation mechanisms. Furthermore, seasonal analysis is more consistent with the independent and identically distributed assumption of extreme value statistics.

Anthropogenic warming has already increased the global mean temperature by 1°C from the pre-industrial level and the current emission trajectory is expected to exceed 1.5°C by the middle of the 21st century (Masson-Delmotte et al., 2018). An increase in global mean temperature increases the water holding capacity of the atmosphere according to the Clausius Clapeyron relationship, which in turn increases the frequency of precipitation extremes (Allan & Soden, 2008; Fowler et al., 2021; Papalexiou & Montanari, 2019; Westra et al., 2014). Our results highlight the human influence on observed daily precipitation extremes across CONUS and emphasize the need for active reduction in human emissions to mitigate the intensification of precipitation extremes in future.

Conflict of Interest

The authors declare no conflicts of interest relevant to this study.

Data Availability Statement

The CPC and CMIP6 multi-model precipitation data used in the study are freely downloadable from https://psl.noaa.gov/data/gridded/data.unified.daily.conus.html and https://pcmdi.llnl.gov/CMIP6/, respectively. The CMIP6 models used in the study are listed in Table S1 in Supporting Information S1. The analysis in this study is performed in R, an open-source computational software. The codes used for the analysis and data visualization are made available at http://www.hydroshare.org/resource/d372565acce441bebdd49a0cf0307ff3.

Acknowledgments

We acknowledge the availability of CPC Unified Gauge-Based Analysis of Daily Precipitation over CONUS data provided by the NOAA PSL, Boulder, Colorado, USA, from their website at https://psl.noaa.gov. We acknowledge the World Climate Research Programme, which, through its Working Group on Coupled Modeling, coordinated and promoted CMIP6. We thank the climate modeling groups for producing and making available their model output, the Earth System Grid Federation (ESGF) for archiving the data and providing access, and the multiple funding agencies who support CMIP6 and ESGF. This work was in part funded by Princeton University. Part of Philippe Naveau's research work was supported by European H2020 XAIDA (Grant agreement ID: 101003469) and the French national programs: 80 PRIME CNRS-INSU, Agence Nationale de la Recherche (ANR) under reference ANR-20-CE40-0025-01 (T-REX), the ANR EXSTA, and the PEPR TRACCS programme under Grant ANR-22-EXTR-0005, and the Mines Paris/INRAE chair Geolearning. The comments by two anonymous reviewers are gratefully acknowledged.

References

Allan, R. P., Barlow, M., Byrne, M. P., Cherchi, A., Douville, H., Fowler, H. J., et al. (2020). Advances in understanding large-scale responses of the water cycle to climate change. *Annals of the New York Academy of Sciences*, *1472*(1), 49–75. https://doi.org/10.1111/nyas.14337

Allan, R. P., & Soden, B. J. (2008). Atmospheric warming and the amplification of precipitation extremes. *Science*, *321*(5895), 1481–1484. https://doi.org/10.1126/science.1160787

Allen, M. (2003). Liability for climate change. *Nature*, *421*(6926), 891–892. https://doi.org/10.1038/421891a

Alonso, A. M., de Zea Bermudez, P., & Scotto, M. G. (2014). Comparing generalized Pareto models fitted to extreme observations: An application to the largest temperatures in Spain. *Stochastic Environmental Research and Risk Assessment*, *28*(5), 1221–1233. https://doi.org/10.1007/s00477-013-0809-8

Beck, H. E., Zimmermann, N. E., McVicar, T. R., Vergopolan, N., Berg, A., & Wood, E. F. (2018). Present and future Köppen-Geiger climate classification maps at 1-km resolution. *Scientific Data*, *5*(1), 1–12. https://doi.org/10.1038/sdata.2018.214

Belzile, L., Wadsworth, J. L., Northrop, P. J., Grimshaw, S. D., Zhang, J., Stephens, M. A., et al. (2015). Package "mev".

Chaussé, P. (2010). Computing generalized method of moments and generalized empirical likelihood with R. *Journal of Statistical Software*, *34–11*(11), 1–35. https://doi.org/10.18637/jss.v034.i11

Coles, S. (2001). Basics of statistical modeling. An introduction to statistical modeling of extreme values (pp. 18–44).

Dai, A. (2006). Precipitation characteristics in eighteen coupled climate models. *Journal of Climate*, *19*(18), 4605–4630. https://doi.org/10.1175/JCLI3884.1

DeMott, C. A., Randall, D. A., & Khairoutdinov, M. (2007). Convective precipitation variability as a tool for general circulation model analysis. *Journal of Climate*, *20*(1), 91–112. https://doi.org/10.1175/JCLI3991.1

Dong, S., Sun, Y., Li, C., Zhang, X., Min, S. K., & Kim, Y. H. (2021). Attribution of extreme precipitation with updated observations and CMIP6 simulations. *Journal of Climate*, *34*(3), 871–881. https://doi.org/10.1175/JCLI-D-19-1017.1

Easterling, D. R., Arnold, J. R., Knutson, T., Kunkel, K. E., LeGrande, A. N., Leung, L. R., et al. (2017). Ch 7. Precipitation change in the United States. *Climate Science Special Report: Fourth National Climate Assessment*, *1*. https://doi.org/10.7930/J0H993CC

Fowler, H. J., Lenderink, G., Prein, A. F., Westra, S., Allan, R. P., Ban, N., et al. (2021). Anthropogenic intensification of short-duration rainfall extremes. *Nature Reviews Earth & Environment 2021*, *2*(2), 107–122. https://doi.org/10.1038/s43017-020-00128-6

Gamet, P., & Jalbert, J. (2022). A flexible extended generalized pareto distribution for tail estimation. *Environmetrics*, *33*(6), e2744. https://doi.org/10.1002/env.2744

Gillett, N. P., Shiogama, H., Funke, B., Hegerl, G., Knutti, R., Matthes, K., et al. (2016). The detection and attribution model intercomparison project (DAMIP v1. 0) contribution to CMIP6. *Geoscientific Model Development*, *9*(10), 3685–3697. https://doi.org/10.5194/gmd-9-3685-2016

Guo, R., Deser, C., Terray, L., & Lehner, F. (2019). Human influence on winter precipitation trends (1921–2015) over North America and Eurasia revealed by dynamical adjustment. *Geophysical Research Letters*, *46*(6), 3426–3434. https://doi.org/10.1029/2018GL081316

Haruna, A., Blanchet, J., & Favre, A.-C. (2023). Modeling intensity-duration-frequency curves for the whole range of non-zero precipitation: A comparison of models. *Water Resources Research*, *59*(6), e2022WR033362. https://doi.org/10.1029/2022wr033362

Hoerling, M., Kumar, A., Dole, R., Nielsen-Gammon, J. W., Eischeid, J., Perlwitz, J., et al. (2013). Anatomy of an extreme event. *Journal of Climate*, *26*(9), 2811–2832. https://doi.org/10.1175/JCLI-D-12-00270.1

Kirchmeier-Young, M. C., Wan, H., Zhang, X., & Seneviratne, S. I. (2019). Importance of framing for extreme event attribution: The role of spatial and temporal scales. *Earth's Future*, *7*(10), 1192–1204. https://doi.org/10.1029/2019EF001253

Kirchmeier-Young, M. C., & Zhang, X. (2020). Human influence has intensified extreme precipitation in North America. *Proceedings of the National Academy of Sciences of the United States of America*, *117*(24), 13308–13313. https://doi.org/10.1073/PNAS.1921628117/SUPPL_FILE/PNAS.1921628117.SAPP.PDF

Legrand, J., Ailliot, P., Naveau, P., & Raillard, N. (2023). Joint stochastic simulation of extreme coastal and offshore significant wave heights. *Annals of Applied Statistics*, *17*(4), 3363–3383. https://doi.org/10.1214/23-aoas1766

Marvel, K., Su, W., Delgado, R., Aarons, S., Chatterjee, A., Garcia, M. E., et al. (2023). Ch. 2. Climate trends. In A. R. Crimmins, C. W. Avery, D. R. Easterling, K. E. Kunkel, B. C. Stewart, & T. K. Maycock (Eds.), *Fifth national climate assessment*. U.S.Global Change Research Program. https://doi.org/10.7930/NCA5.2023.CH2

Masson-Delmotte, V. P. Z., Pörtner, H.-O., Roberts, D., Skea, J., Shukla, P. R., Pirani, A., et al. (2018). IPCC, 2018: Summary for policymakers. In *Global Warming of 1.5°C. An IPCC Special Report on the impacts of global warming of 1.5°C above pre-industrial levels and related global greenhouse gas emission pathways, in the context of strengthening the global*. Global Warming of 1.5°C. https://doi.org/10.1017/9781009157940.001

Myhre, G., Alterskjær, K., Stjern, C. W., Hodnebrog, Ø., Marelle, L., Samset, B. H., et al. (2019). Frequency of extreme precipitation increases extensively with event rareness under global warming. *Scientific Reports*, *9*(1), 16063. https://doi.org/10.1038/s41598-019-52277-4

Na, Y., Fu, Q., Leung, L. R., Kodama, C., & Lu, R. (2022). Mesoscale convective systems simulated by a high-resolution global nonhydrostatic model over the United States and China. *Journal of Geophysical Research: Atmospheres*, *127*(7), 1–21. https://doi.org/10.1029/2021JD035916

Naveau, P., Hannart, A., & Ribes, A. (2020). Statistical methods for extreme event attribution in climate science. *Annual Review of Statistics and Its Application*, *7*(1), 89–110. https://doi.org/10.1146/annurev-statistics-031219-041314

Naveau, P., Huser, R., Ribereau, P., & Hannart, A. (2016). Modeling jointly low, moderate, and heavy rainfall intensities without a threshold selection. *Water Resources Research*, *52*(4), 2753–2769. https://doi.org/10.1002/2015WR018552

Nerantzaki, S. D., Papalexiou, S. M., Rajulapati, C. R., & Clark, M. P. (2023). Nonstationarity in high and low-temperature extremes: Insights from a global observational data set by merging extreme-value methods. *Earth's Future*, *11*(11), e2023EF003506. https://doi.org/10.1029/2023EF003506

van Oldenborgh, G. J., van der Wiel, K., Kew, S., Philip, S., Otto, F., Vautard, R., et al. (2021). Pathways and pitfalls in extreme event attribution. *Climatic Change*, *166*(1), 1–27. https://doi.org/10.1007/S10584-021-03071-7

Paciorek, C. J., Stone, D. A., & Wehner, M. F. (2017). Quantifying statistical uncertainty in the attribution of human influence on severe weather. http://arxiv.org/abs/1706.03388

Pall, P., Patricola, C. M., Wehner, M. F., Stone, D. A., Paciorek, C. J., & Collins, W. D. (2017). Diagnosing conditional anthropogenic contributions to heavy Colorado rainfall in September 2013. *Weather and Climate Extremes*, *17*, 1–6. https://doi.org/10.1016/j.wace.2017.03.004

Papalexiou, S. M., & Montanari, A. (2019). Global and regional increase of precipitation extremes under global warming. *Water Resources Research*, *55*(6), 4901–4914. https://doi.org/10.1029/2018wr024067

Philip, S., Kew, S., van Oldenborgh, G. J., Otto, F., Vautard, R., van der Wiel, K., et al. (2020). A protocol for probabilistic extreme event attribution analyses. *Advances in Statistical Climatology, Meteorology and Oceanography*, *6*(2), 177–203. https://doi.org/10.5194/ASCMO-6-177-2020

Risser, M. D., Collins, W. D., Wehner, M. F., O'Brien, T. A., Paciorek, C. J., O'Brien, J. P., et al. (2022). A framework for detection and attribution of regional precipitation change: Application to the United States historical record. *Climate Dynamics*, *60*(3–4), 705–741. https://doi.org/10.1007/s00382-022-06321-1

Rivoire, P., Martius, O., & Naveau, P. (2021). A comparison of moderate and extreme ERA-5 daily precipitation with two observational data sets. *Earth and Space Science*, *8*(4), e2020EA001633. https://doi.org/10.1029/2020EA001633

Seneviratne, S. I., Zhang, X., Adnan, M., Badi, W., Dereczynski, C., Di Luca, A., et al. (2021). Weather and Climate Extreme Events in a Changing Climate. *Climate Change 2021: The Physical Science Basis*. Contribution of Working Group I to the Sixth Assessment Report of the Intergovernmental Panel on Climate Change. https://doi.org/10.1017/9781009157896.013

Serinaldi, F., & Kilsby, C. G. (2014). Rainfall extremes: Toward reconciliation after the battle of distributions. *Water Resources Research*, *50*(1), 336–352. https://doi.org/10.1002/2013WR014211

Srivastava, A., Grotjahn, R., & Ullrich, P. A. (2020). Evaluation of historical CMIP6 model simulations of extreme precipitation over contiguous US regions. *Weather and Climate Extremes*, *29*, 100268. https://doi.org/10.1016/j.wace.2020.100268

Trenberth, K. E. (2018). Climate change caused by human activities is happening and it already has major consequences. In *Journal of energy and natural resources law*. Taylor and Francis Ltd. https://doi.org/10.1080/02646811.2018.1450895

Van Der Wiel, K., Kapnick, S. B., Jan Van Oldenborgh, G., Whan, K., Philip, S., Vecchi, G. A., et al. (2017). Rapid attribution of the August 2016 flood-inducing extreme precipitation in south Louisiana to climate change. *Hydrology and Earth System Sciences*, *21*(2), 897–921. https://doi.org/10.5194/hess-21-897-2017

Wang, H., & Asefa, T. (2024). Enhanced performance of CMIP6 climate models in simulating historical precipitation in the Florida Peninsula. *International Journal of Climatology*, *44*(8), 2758–2778. https://doi.org/10.1002/joc.8479

Wang, S. Y. S., Zhao, L., Yoon, J. H., Klotzbach, P., & Gillies, R. R. (2018). Quantitative attribution of climate effects on Hurricane Harvey's extreme rainfall in Texas. *Environmental Research Letters*, *13*(5), 054014. https://doi.org/10.1088/1748-9326/AABB85

Wehner, M., & Sampson, C. (2021). Attributable human-induced changes in the magnitude of flooding in the Houston, Texas region during Hurricane Harvey. *Climatic Change*, *166*(1–2), 1–13. https://doi.org/10.1007/S10584-021-03114-Z/TABLES/2

Westra, S., Fowler, H. J., Evans, J. P., Alexander, L. V., Berg, P., Johnson, F., et al. (2014). Future changes to the intensity and frequency of short-duration extreme rainfall. *Reviews of Geophysics*, *52*(3), 522–555. https://doi.org/10.1002/2014RG000464

Zhao, W. S.-Y., Zhao, L., Yoon, J.-H., Klotzbach, P., & Gillies, R. R. (2018). Quantitative attribution of climate effects on Hurricane Harvey's extreme rainfall in Texas. *Environmental Research Letters*, *13*(5), 054014. https://doi.org/10.1088/1748-9326/aabb85

References From the Supporting Information

Bi, D., Dix, M., Marsland, S., O'End-centuryrell, S., Sullivan, A., Bodman, R., et al. (2020). Configuration and spin-up of ACCESS-CM2, the new generation Australian community climate and earth system simulator coupled model. *Journal of Southern Hemisphere Earth Systems Science*, *70*(1), 225–251. https://doi.org/10.1071/ES19040

Boucher, O., Servonnat, J., Albright, A. L., Aumont, O., Balkanski, Y., Bastrikov, V., et al. (2020). Presentation and evaluation of the IPSL-CM6A-LR climate model. *Journal of Advances in Modeling Earth Systems*, *12*(7), e2019MS002010. https://doi.org/10.1029/2019MS002010

Danabasoglu, G., Lamarque, J. F., Bacmeister, J., Bailey, D. A., DuVivier, A. K., Edwards, J., et al. (2020). The community earth system model version 2 (CESM2). *Journal of Advances in Modeling Earth Systems*, *12*(2), e2019MS001916. https://doi.org/10.1029/2019ms001916

Dunne, J. P., Horowitz, L. W., Adcroft, A. J., Ginoux, P., Held, I. M., John, J. G., et al. (2020). The GFDL Earth System Model version 4.1 (GFDL-ESM 4.1): Overall coupled model description and simulation characteristics. *Journal of Advances in Modeling Earth Systems*, *12*(11), e2019MS002015. https://doi.org/10.1029/2019ms002015

Golaz, J.-C., Van Roekel, L. P., Zheng, X., Roberts, A. F., Wolfe, J. D., Lin, W., et al. (2022). The DOE E3SM Model Version 2: Overview of the physical model and initial model evaluation. *Journal of Advances in Modeling Earth Systems*, *14*(12), e2022MS003156. https://doi.org/10.1029/2022MS003156

Li, L., Yu, Y., Tang, Y., Lin, P., Xie, J., Song, M., et al. (2020). The flexible global ocean-atmosphere-land system model grid-point version 3 (FGOALS-g3): Description and evaluation. *Journal of Advances in Modeling Earth Systems*, *12*(9), e2019MS002012. https://doi.org/10.1029/2019ms002012

Lu, Y., Wu, T., Li, Y., & Yang, B. (2021). Mitigation of the double ITCZ syndrome in BCC-CSM2-MR through improving parameterizations of boundary-layer turbulence and shallow convection. *Geoscientific Model Development*, *14*(8), 5183–5204. https://doi.org/10.5194/GMD-14-5183-2021

Seland, Ø., Bentsen, M., Olivié, D., Toniazzo, T., Gjermundsen, A., Graff, L. S., et al. (2020). Overview of the Norwegian Earth System Model (NorESM2) and key climate response of CMIP6 DECK, historical, and scenario simulations. *Geoscientific Model Development*, *13*(12), 6165–6200. https://doi.org/10.5194/GMD-13-6165-2020

Swart, N. C., Cole, J. N. S., Kharin, V. V., Lazare, M., Scinocca, J. F., Gillett, N. P., et al. (2019). The Canadian earth system model version 5 (CanESM5.0.3). *Geoscientific Model Development*, *12*(11), 4823–4873. https://doi.org/10.5194/GMD-12-4823-2019

Tatebe, H., Ogura, T., Nitta, T., Komuro, Y., Ogochi, K., Takemura, T., et al. (2019). Description and basic evaluation of simulated mean state, internal variability, and climate sensitivity in MIROC6. *Geoscientific Model Development*, *12*(7), 2727–2765. https://doi.org/10.5194/GMD-12-2727-2019

Yukimoto, S., Kawai, H., Koshiro, T., Oshima, N., Yoshida, K., Urakawa, S., et al. (2019). The meteorological research institute Earth system model version 2.0, MRI-ESM2.0: Description and basic evaluation of the physical component. *Journal of the Meteorological Society of Japan*, *97*(5), 931–965. https://doi.org/10.2151/jmsj.2019-051

Ziehn, T., Chamberlain, M. A., Law, R. M., Lenton, A., Bodman, R. W., Dix, M., et al. (2020). The Australian earth system model: ACCESS-ESM1.5. *Journal of Southern Hemisphere Earth Systems Science*, *70*(1), 193–214. https://doi.org/10.1071/ES19035